Predicting Frictional Properties of Graphene Kirigami Using Molecular Dynamics and Neural Networks

Designs for a negative friction coefficient.

Mikkel Metzsch Jensen

Thesis submitted for the degree of
Master in Computational Science: Materials Science
60 credits

Department of Physics
Faculty of mathematics and natural sciences

UNIVERSITY OF OSLO

Spring 2023

Predicting Frictional Properties of Graphene Kirigami Using Molecular Dynamics and Neural Networks

Designs for a negative friction coefficient.

Mikkel Metzsch Jensen

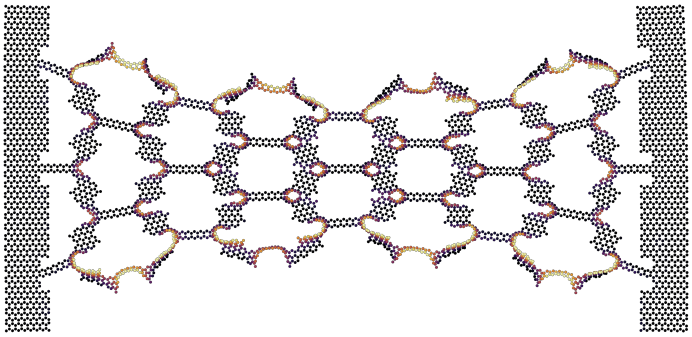

Predicting Frictional Properties of Graphene Kirigami Using Molecular Dynamics and Neural Networks

http://www.duo.uio.no/

Printed: Reprosentralen, University of Oslo

Abstract

Basic introduction

Various theoretical models and experimental results propose different governing mechanisms for friction at the nanoscale.

More detailed background

We consider a graphene sheet modified with Kirigami-inspired cuts and under the influence of strain. Prior research has demonstrated that this system exhibits out-of-plane buckling, which could result in a decrease in contact area when sliding on a substrate. According to asperity theory, this decrease in contact area is expected to lead to a reduction of friction.

General problem

However, to the best of our knowledge, no previous studies have investigated the friction behavior of a nanoscale Kirigami graphene sheet under strain.

Summarize main result: "here we show"

Here we show that specific Kirigami designs yield a non-linear dependency between kinetic friction and the strain of the sheet.

General context

Using molecular dynamics simulation, we have found a non-monotonic increase in friction with strain. We found that the friction-strain relationship does not show any clear dependency on contact area which contradicts asperity theory. Our findings suggest that the effect is associated with the out-of-plane buckling of the graphene sheet and we attribute this to a commensurability effect. By mimicking a load-strain coupling through tension, we were able to utilize this effect to demonstrate a negative friction coefficient on the order of -0.3 for loads in the range of a few nN. In addition, we have attempted to use machine learning to capture the relationship between Kirigami designs, load, and strain, with the objective of performing an accelerated search for new designs. While this approach produced some promising results, we conclude that further improvements to the dataset are necessary in order to develop a reliable model.

Broader perspective

We anticipate our findings to be a starting point for further investigations of the underlying mechanism for the frictional behavior of a Kirigami sheet. For instance, the commensurability hypothesis could be examined by varying the sliding angle in simulations. We propose to use an active learning strategy to extend the dataset for the use of machine learning to assist these investigations. If successful, further studies can be done on the method of inverse design. In summary, our findings suggest that the application of nanoscale Kirigami can be promising for developing novel friction-control strategies.

353 words

Various numerical models and experimental results propose different governing mechanisms for friction at the nanoscale. We consider a graphene sheet modified with Kirigami-inspired cuts and under the influence of strain. Prior research has demonstrated that this system exhibits out-of-plane buckling, which could result in a decrease in contact area when sliding on a substrate. According to asperity theory, this decrease in contact area is expected to lead to a reduction of friction. However, to the best of our knowledge, no previous studies have investigated the friction behavior of a nanoscale Kirigami graphene sheet under strain. Here we show that specific Kirigami designs yield a non-linear dependency between kinetic friction and the strain of the sheet. Using molecular dynamics simulation, we have found a non-monotonic increase in friction with strain. We found that the friction-strain relationship does not show any clear dependency on contact area which contradicts asperity theory. Our findings suggest that the effect is associated with the out-of-plane buckling of the graphene sheet and we attribute this to a commensurability effect. By mimicking a load-strain coupling through tension, we were able to utilize this effect to demonstrate a negative friction coefficient on the order of -0.3 for loads in the range of a few nN. In addition, we have attempted to use machine learning to capture the relationship between Kirigami designs, load, and strain, with the objective of performing an accelerated search for new designs. While this approach produced some promising results, we conclude that further improvements to the dataset are necessary in order to develop a reliable model. We anticipate our findings to be a starting point for further investigations of the underlying mechanism for the frictional behavior of a Kirigami sheet. For instance, the commensurability hypothesis could be examined by varying the sliding angle in simulations. We propose to use an active learning strategy to extend the dataset for the use of machine learning to assist these investigations. If successful, further studies can be done on the method of inverse design. In summary, our findings suggest that the application of nanoscale Kirigami can be promising for developing novel friction-control strategies.

Acknowledgments

The task of writing a master's thesis is a demanding and extensive project which I could not have been done without the support of many good people around me. First of all, I want to thank my supervisors Henrik Andersen Sveinsson and Anders Malthe-Sørenssen for the assistance in this thesis work. I am especially grateful for the weekly meetings with Henrik and the inspiring discussion being had as we unraveled the discoveries related to the topic of this thesis. I remember that I initially asked for an estimate of how much time he had available for supervision and the answer was something along the lines of "There are no limits really, just send me an email and we figure it out". This attitude captures the main experience I have had working with Henrik and I am profoundly grateful for the time and effort you have put into this project. I hope that you do not regret said statement, too much, because I have certainly been taken advantage of it. I also want to thank Even Marius Nordhagen for technical support regarding the use of the computational cluster, in times when the computer did exactly what it was told and was being silly. In that context, I also want to acknowledge the University of Oslo (CCSE?) for making these resources available.

I would like to express my gratitude to all the parties involved in making it possible for me to write my thesis from Italy. I am particularly grateful for the flexibility shown by my supervisors and for the support of Anders Kvellestad, who allowed me to work remotely as a group teacher. I would also like to thank Scuola Normale Superiore for providing me with access to their library.

I realize that it is a commonly used cliche to express gratitude for the support of loved ones. However, I want to highlight the exceptional role played by my fiancé, Ida. She deserves the main credit for helping me maintain a healthy state of mind, and she has provided me with a solid foundation for a fulfilling life that enables me to pursue secondary objectives, such as an academic career. I look forward to spending the rest of my life with you.

Throughout this thesis, I have used a formal "we" mainly as a customary habit related to the formalities of scientific writing in a team. However, I have come to the realization that this approach feels more appropriate since I have not been working on this project alone. I have found support all the way from colleagues and friends at the University of Oslo, to my family residing in Denmark, and my life partner sleeping beside me every night here in Italy. They constitute the "good people around me" who have made this thesis possible.

List of Symbols

F_N Normal force (normal load)

Acronyms

FFM Friction Force Microscopes. 7

GAN Generative Adversarial Networks. 2, 23

LJ Lennard-Jones. 7, 8, 9, 10

MD Molecular Dynamics. 1, 2, 3, 4, 7, 8, 14, 16, 19, 20, 21, 22

ML Machine Learning. 2

Contents

Chapter 1

Introduction

1.1 Motivation

Friction is the force that prevents the relative motion of objects in contact. From our everyday life, we recognize it as the inherent resistance to sliding motion. Some surfaces appear slippery and some rough, and we know intuitively that sliding down a snow-covered hill is much more exciting than its grassy counterpart. Without friction, it would not be possible to walk across a flat surface, lean against the wall without falling over or secure an object by the use of nails or screws [p. 5] [1]. It is probably safe to say that the concept of friction is integrated into our everyday life to such an extent that most people take it for granted. However, the efforts to control friction date back to the early civilization (3500 B.C.) with the use of the wheel and lubricants to reduce friction in translational motion [2]. Today, friction is considered a part of the wider field *tribology* derived from the Greek word *tribos* meaning "rubbing" and includes the science of friction, wear and lubrication [2]. The most compelling motivation to study tribology is ultimately to gain full control of friction and wear for various technical applications. Especially, reducing friction is of great interest as this has advantages for energy efficiency. It has been reported that tribological problems have a significant potential for economic and environmental improvements [3]:

> "On global scale, these savings would amount to 1.4% of the GDP annually and 8.7% of the total energy consumption in the long term." [4].

On the other hand, the reduction of friction is not the only sensible application for tribological studies. Controlling frictional properties, besides minimization, might be of interest in the development of a grasping robot where finetuned object handling is required. While achieving a certain "constant" friction response is readily obtained through appropriate material choices, we are yet to unlock the full capabilities to alter friction dynamically on the go. One example from nature inspiring us to think along these lines are the gecko feet. More precisely, the Tokay gecko has received a lot of attention in scientific studies aiming to unravel the underlying mechanism of its "togglable" adhesion properties. Although geckos can produce large adhesive forces, they retain the ability to remove their feet from an attachment surface at will [5]. This makes the gecko able to achieve a high adhesion on the feet when climbing a vertical surface while lifting them for the next step remains relatively effortless. For a grasping robot, we might consider an analog frictional concept of a surface material that can change from slippery to rough on demand depending on specific tasks; Slippery and smooth when interacting with people and rough and firmly gripping when moving heavy objects.

In recent years an increasing amount of interest has gone into the studies of the microscopic origin of friction, due to the increased possibilities in surface preparation and the development of nanoscale experimental methods. Nano-friction is also of great concern for the field of nano-machining where the frictional properties between the tool and the workpiece dictate machining characteristics [3]. With concurrent progress in computational capacity and development of Molecular Dynamics (MD), numerical investigations serve as an invaluable tool for getting insight into the nanoscale mechanics associated with friction. This simulation-based approach can be considered as a "numerical experiment" enabling us to create and probe a variety of high-complexity systems which are still out of reach for modern experimental methods.

In materials science such MD-based numerical studies have been used to explore the concept of so-called *metamaterials* where the material compositions are designed meticulously to enhance certain physical properties [6–11]. This is often achieved either by intertwining different material types or removing certain regions completely. In recent papers by Hanakata et al. [6, 7], numerical studies have showcased that the mechanical properties of a graphene sheet, yield stress and yield strain, can be altered through the introduction of so-called *Kirigami* inspired cuts into the sheet. Kirigami is a variation of origami where the paper is cut additionally to being folded. While these methods originate as an art form, aiming to produce various artistic objects, they have proven to be applicable in a wide range of fields such as optics, physics, biology, chemistry and engineering [12]. Various forms of stimuli enable direct 2D to 3D transformations through folding, bending, and twisting of microstructures. While original human designs have contributed to specific scientific applications in the past, the future of this field is highly driven by the question of how to generate new designs optimized for certain physical properties. However, the complexity of such systems and the associated design space makes for seemingly intractable[1] problems ruling out analytic solutions.

Earlier architecture design approaches such as bioinspiration, looking at gecko feet for instance, and Edisonian, based on trial and error, generally rely on prior knowledge and an experienced designer [9]. While the Edisonian approach is certainly more feasible through numerical studies than real-world experiments, the number of combinations in the design space rather quickly becomes too large for a systematic search, even when considering the computation time on modern-day hardware. However, this computational time constraint can be relaxed by the use of machine learning (ML) which has proven successful in the establishment of a mapping from the design space to physical properties of interest. This gives rise to two new styles of design approaches: One, by utilizing the prediction from a trained network we can skip the MD simulations altogether resulting in an *accelerated search* of designs. This can be further improved by guiding the search accordingly to the most promising candidates, for instance, as done with the *genetic algorithm* based on mutation and crossing of the best candidates so far. Another more sophisticated approach is through generative methods such as *Generative Adversarial Networks* (GAN) or diffusion models. The latter is being used in state-of-the-art AI systems such as OpenAI's DALL·E2 [13] or Midjourney [14]. By working with a so-called *encoder-decoder* network structure, one can build a model that reverses the prediction process. This is often referred to as *reverse design*, where the model predicts a design from a set of physical target properties. In the papers by Hanakata et al. [6, 7] both the *accelerated search* and the *inverse design* approach was proven successful to create novel metamaterial Kirigami designs with the graphene sheet.

Hanakata et al. attributes the variation in mechanical properties to the non-linear effects arising from the out-of-plane buckling of the sheet. Since it is generally accepted that the surface roughness is of great importance for frictional properties it can be hypothesized that Kirigami-induced out-of-plane buckling can also be exploited for the design of frictional metamaterials. For certain designs, we might hope to find a relationship between the stretching of the sheet and frictional properties. If significant, this could give rise to an adjustable friction behavior beyond the point of manufacturing. For instance, the grasping robot might apply such a material as artificial skin for which stretching or relaxing of the surface could result in a changeable friction strength.

In addition, the Kirigami graphene properties can be explored through a potential coupling between the stretch and the normal load, through a nanomachine design, with the aim of altering the friction coefficient. This invites the idea of non-linear friction coefficients which might in theory also take on negative values. The latter would constitute a rare property only found a few cases. These are mainly for the unloading phase of adhesive surfaces [15] or the loading phase of particular heterojunction materials [16, 17].

To the best of our knowledge, Kirigami has not yet been implemented to alter the frictional properties of a nanoscale system. However, in a recent paper by Liefferink et al. [18] it is reported that macroscale Kirigami can be used to dynamically control the macroscale roughness of a surface through stretching. They reported that the roughness change led to a changeable frictional coefficient by more than one order of magnitude. This supports the idea that Kirigami designs can be used to alter friction, but we believe that taking this concept to the nanoscale would involve a different set of governing mechanisms and thus contribute to new insight in this field.

[1] In computer science we define an *intractable* problem as a problem with no *efficient* algorithm to solve it nor any analytical solutions. The only way to solve such problems is the *brute-force* approach, simply trying all possible solutions, which is often beyond the capabilities of computational resources.

1.2 Goals

In this thesis, we investigate the prospects of altering the frictional properties of a graphene sheet through the application of Kirigami-inspired cuts and stretching of the sheet. With the use of molecular dynamics (MD) simulations, we evaluate the frictional properties of various Kirigami designs under different physical conditions. Based on the MD results, we investigate the possibility to use machine learning for the prediction of frictional properties and subsequently using the model for an accelerated search of new designs. The main goals of the thesis can be summarized as follows.

1. Design an MD simulation procedure to evaluate the frictional properties of a Kirigami graphene sheet under specified physical conditions.

2. Develop a numerical framework to generate various Kirigami designs, both by seeking inspiration from macroscale designs and by the use of a random walk based algorithm.

3. Investigate the frictional behavior under varying load and stretch for different Kirigami designs.

4. Develop and train a machine learning model to predict the MD simulation result and perform an accelerated search of new designs with the scope of optimizing certain frictional properties.

1.3 Contributions

By working towards the goals outlined above (Sec. 1.2), I have discovered a non-linear relationship between the kinetic friction and the strain for certain Kirigami patterns. This phenomenon was found to be associated with the out-of-plane buckling of the Kirigami sheet but with no clear relationship to the contact area or the tension in the sheet. I found that this method does not provide any mechanism for a reduction in friction, in comparison to a non-cut sheet, but the straining of certain Kirigami sheets allows for a non-monotonic increase in friction. The relationship to normal load was proven negligible in this context and I have demonstrated that a coupled system of load and strain (through sheet tension) can exhibit a negative friction coefficient in certain load ranges. Moreover, I have created a dataset of roughly 10,000 data points for assessing the employment of machine learning and accelerated search of Kirigami designs. I have found, that this approach might be useful, but it requires an extended dataset in order to produce reliable results for a search of new designs.

During our investigations, I have built three numerical tools, beyond the regular scripts associated with data analysis, which can be found on Github [19]. The tools are summarized in the following.

- I have written a LAMMPS-based [20] tool for simulating and measuring the frictional properties of a graphene sheet sliding on a substrate. The code is generally made flexible concerning the choice of sheet configuration, system size, simulation parameters and MD potentials, which makes it applicable for further studies within this topic. I have also built an automized procedure to carry out multiple simulations under varying parameters by submitting jobs to a computational cluster via an ssh connection. This was done by adding minor additions to the python package developed by E. M. Nordhagen [21].

- I have generated a Python-based tool for generating Kirigami patterns and exporting these in a compatible format with the simulation software. The generation of molecular structures is done with the use of ASE [22]. Our software includes two classes of patterns inspired by macroscale designs and a random walk algorithm which allow for a variety of different designs through user-defined biases and constraints. Given our system size of choice, the first two pattern generators are capable of generating on the order of 10^8 unique designs while the random walk generator allows for significantly more.

- I have built a machine learning tool based on Pytorch [23] which includes setting up the data loaders, a convolutional network architecture, a loss function, and general algorithms for training and validating the results. Additionally, I have written several scripts for performing grid searches and analyzing the model predictions in the context of the frictional properties of graphene.

All numerical implementations used for this thesis have been originally developed for the purpose with the exception of the usage of libraries as mentioned above and commonly known Python libraries such as Numpy and Matplotlib.

1.4 Thesis structure

The thesis is divided into two parts. In Part I we introduce the relevant theoretical background, and in Part II we present the numerical implementations and the results of this thesis.

Part I contains a description of the theoretical background related to Friction (**??**), Molecular Dynamics (Chapter 2) and Machine Learning (**??**). In **??** we fill formulate our research questions n the light of the friction theory.

In Part II, we begin by presenting our definition and setting up of the systemm in **??**. This includes the MD simulations and the generation of Kirigami designs. This is followed by a pilot study in **??** where we evaluate the simulation results for various physical conditions and compare a non-cut sheet to two different Kirigami designs. Further explorations of the Kirigami configurations are carried out in **??** which includes the generation of a dataset and the employment of machine learning and an accelerated search. We use the results from the pilot study to demonstrate the possibility to achieve a negative friction coefficient for a system with coupled load and strain in **??**. Finally, we summarize our results and provide an outlook for further studies in Chapter 3. Additional figures are shown in **??**, **??** and **??**.

Part I

Background Theory

Chapter 2

Molecular Dynamics

Molecular Dynamics (MD) is an atomistic simulation method that is commonly employed in the investigation of atomic-scale friction due to its ability to track each atom in a system [24]. In recent years, advances in computing algorithms and hardware have made MD simulations increasingly capable of simulating tribological systems [25]. We will utilize MD as our primary numerical approach to examine the frictional behavior of a nanoscale Kirigami sheet sliding on a substrate. The small-scale modifications associated with nanoscale Kirigami are still beyond the reach of experimental approaches, and the complexity of the system precludes analytical solutions as well. Hence, MD simulations represent one of the few viable options for addressing this problem.

An MD simulation can be viewed as a "computational experiment", where we specify a set of initial conditions and evolve the system to measure certain properties of interest. This is done through the definition of interatomic force fields which allow us to solve Newton's equation of motion by numerical integration [26, p. 303]. Other more sophisticated and accurate approaches exist, like ab initio MD which utilizes electronic structure calculations at simulation time [27]. One of the most popular methods is based on density functional theory (DFT) [28] which considers quantum mechanical modeling of the electronic state of the system. However, such methods are rarely used in sliding friction simulations since the computational cost makes it only feasible to handle relatively small systems, typically hundreds of atoms, for relatively short durations, typically much less than 1 ns [29]. In addition, we aim to perform multiple simulations under the change of various physical parameters which adds extra demands on the computational resources.

In this chapter, we introduce the fundamental principles of MD modeling and describe our implementation choices for the system of interest. We will focus on the key aspects related to our implementation rather than providing a comprehensive analysis of all available techniques.

2.1 Potentials

The interatomic force fields governing the MD simulation are given from the choice of potentials and have a significant impact on the outcomes obtained. The potentials can vary from intricate energy surfaces that consider electrons at either the density-functional or tight-binding level to angle-dependent many-particle potentials, basic pairwise potentials, or simple models of elastic springs, and extensions of Frenkel-Kontorova-type formulations [29]. For the choice of potentials, and materials, we take a basis in the numerical MD study by Li et al. [30] simulating a FFM type setup where a silicon tip indents a graphene sheet supported by a silicon substrate. Our system obviously differs from this arrangement since we will be sliding the entire sheet upon the substrate. Nevertheless, we contend that this serves as an appropriate basis for selecting the potentials based on the materials involved. Thus, we adopt the potentials from [30] describing the covalent bonds between carbon atoms (C–C) in the graphene sheet with the Tersoff potential and the covalent bonds between silicon atoms (Si–Si) in the substrate with the Stillinger–Weber potential. A typical 12–6 Lennard–Jones (LJ) potential is used to describe the van der Waals adhesive interaction between the graphene sheet and the substrate.

2.1.1 General formulation of potentials

The potentials determine the interatomic forces in the MD simulation, with the force F acting on an atom being derived from the potential energy U as the derivative $\mathbf{F} = -\nabla U$, where $\nabla = (\frac{\partial}{\partial x}, \frac{\partial}{\partial y}, \frac{\partial}{\partial z})$. The energy of N

interacting particles can be described as an expansion in terms of participating atoms as

$$U = \sum_i V_1(\mathbf{r}_i) + \sum_{\substack{i,j \\ i<j}} V_2(\mathbf{r}_i, \mathbf{r}_j) + \sum_{\substack{i,j,k \\ i<j<k}} V_3(\mathbf{r}_i, \mathbf{r}_j, \mathbf{r}_i) + \cdots ,$$

where $\mathbf{r}_n$ is the position of the n^{th} particle and V_m is called an m-body potential [31]. The first one-body term corresponds to an external potential (e.g. gravity), followed by the two-body term, the three-body term and so on. The simplest model that includes particle interaction is the pair potential truncating the expansion after the two-body term. A general feature of the pair potentials is that they favor close-packed structures that are unsuited to describe covalent bonds which take more open structures. In particular, pair potentials are completely inapplicable to strongly covalent systems [31]. In order to accommodate the description of covalent bonds we include the three-body term in both the Stillinger–Weber and Tersoff potential. For the interaction between the sheet and the substrate, we use the LJ pair potential describing the non-bonded van der Waals interaction which is often used to treat interactions between surfaces in friction simulations [3, 32–34]. In the following sections Sec. 2.1.2 to 2.1.4 we will introduce each of the potentials in more detail.

2.1.2 Lennard Jones

The theoretical basis in section is based on [35–37]. The Lennard-Jones (LJ) model is one of the most commonly used pair potentials for MD simulations. LJ models the potential energy between two non-bonding atoms solely based on interatomic distance. The model accounts for long-ranged attractive forces arising from London dispersion forces (dipole-induced dipole) and repulsive forces that capture the hard core of overlapping electron orbitals at small distances (Pauli repulsion). Thus, it assumes neutrally charged atoms and was originally proposed for noble gases. The classical 12–6 version of the model, referring to the powers of the repulsive and attractive forces respectively, reads

$$U = 4\epsilon \left[\left(\frac{\sigma}{r}\right)^{12} - \left(\frac{\sigma}{r}\right)^{6} \right], \qquad r < r_c, \tag{2.1}$$

where r is the interatomic distance with cut-off r_c, ϵ is the depth of the potential well and σ the interatomic distance where the the potential is zero. The potential is illustrated in Fig. 2.1. By solving for the potential minimum ($dU/dr = 0$) we find the equilibrium distance to be $r_0 = \sigma 2^{1/6}$. This makes for a slightly more intuitive interpretation of σ as the parameter which sets the equilibrium distance between atoms, i.e. the dividing line for which the force is repulsive or attractive. We will adopt the potential parameters from Li et al. [30] with $\sigma = 3.0\,\text{Å}$ and $\epsilon = 0.0092\,\text{eV}$.

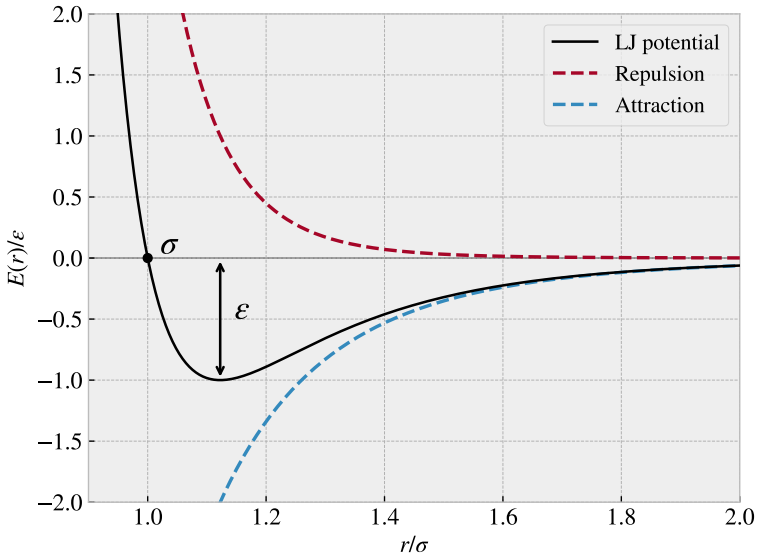

Figure 2.1: Illustration of the LJ potential Eq. (2.1) showing the contributions from the repulsive and attractive part of the potential.

2.1.3 Stillinger-Weber

The theoretical background of this section is based on [38, 39]. The Stillinger-Weber potential takes the form of a three-body potential

$$U = \sum_i \sum_{j>i} \phi_2(r_{ij}) + \sum_i \sum_{j\neq i} \sum_{k>j} \phi_3(r_{ij}, r_{ik}, \theta_{ijk}),$$

where r_{ij} denotes the distance between atom i and j, and θ_{ijk} the angle between bond ij and jk (see Fig. 2.2). The summation is over all neighbors j and k of atom i within a cut-off distance $r = a\sigma$.

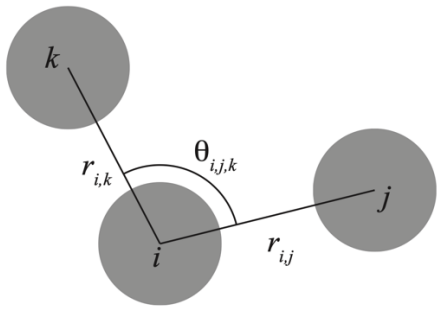

Figure 2.2: Illustration showing the notation for the distances r_{ik} and r_{ij} and the angle θ_{ijk} in consideration to the atoms i, j and k.

The two-body term ϕ_2 builds from the LJ model with the addition of an exponential cutoff term

$$\phi_2(r_{ij}) = A_{ij}\epsilon_{ij}\left[B_{ij}\left(\frac{\sigma_{ij}}{r_{ij}}\right)^{p_{ij}} - \left(\frac{\sigma_{ij}}{r_{ij}}\right)^{q_{ij}}\right]\exp\left(\frac{\sigma_{ij}}{r_{ij} - a_{ij}\sigma_{ij}}\right). \tag{2.2}$$

The model parameters A, ϵ, B, σ, p, q and a come with i, j indices to indicate that these parameters should be specified for each unique pair of atom types. However, in our case, we will only provide a single value for each model parameter since we are exclusively dealing with Si–Si bonds. We see that the first term in Eq. (2.2) is reminiscent of the LJ model in Eq. (2.1) while the last term effectively drives the potential to zero at $r = a\sigma$, which is the chosen cut-off distance for the potential evaluation. With the chosen model parameters for the Si–Si modeling (see Table 2.1), the cut-off becomes $\sim 3.8\,\text{Å}$. The three body term includes an angle dependency as

$$\phi_3(r_{ij}, r_{ik}, \theta_{ijk}) = \lambda_{ijk}\ \epsilon_{ijk}\left[\cos\theta_{ijk} - \cos\theta_{0,ijk}\right]^2 \exp\left(\frac{\gamma_{ij}\sigma_{ij}}{r_{ij} - a_{ij}\sigma_{ij}}\right)\exp\left(\frac{\gamma_{ik}\sigma_{ik}}{r_{ik} - a_{ik}\sigma_{ik}}\right), \tag{2.3}$$

where $\theta_{0,ijk}$ is the equilibrium angle. The first term of Eq. (2.3) includes an angle dependency analog to a harmonic oscillator based on a cosine angle distance from the equilibrium angle. The final two terms act again as a cut-off function by driving the potential to zero at $r_{ij} = a_{ij}\sigma_{ij}$ and $r_{ik} = a_{ik}\sigma_{ik}$ respectively. We adopt the parameters for Si–Si modelling suggested in the original paper by Stillinger and Weber [39] which is shown in Table 2.1 along with an interpretation of each model parameter.

Table 2.1: Parameters for the Stilliner-Weber potential used for intermolecular interactions in the silicon substrate. The parameters are adopted from [39].

Parameter	Value	Description
ϵ	2.1683 eV	Depth of the potential well for each pair and triplets of atom types.
σ	2.0951 Å	Distance for which the individual pair interactions has zero potential (analog to the LJ model).
a	1.80	The cut-off distance for each pair of atom types in units of σ.
λ	21.0	The overall depth of the three-body potential well.
γ	1.20	The shape of the three-body cut-off terms.
$\cos(\theta_0)$	-1/3	Cosine of equilibrium angle.
A	7.049556277	The overall depth of the two-body potential well.
B	0.6022245584	Scales the repulsion part of the two-body term.
p	4.0	The power dependency for the repulsion part of the two-body term.
q	0.0	The power dependency for the attraction part of the two-body term.
tol	0	(LAMMPS specific) Option to define a different cut-off than the theoretical $r = a\sigma$. tol = 0 refers to the use of the theoretical cut-off.

2.1.4 Tersoff

The theoretical basis in this section is based on [31, 40]. The Tersoff potential abandons the idea of a general m-body form and attempts instead to build the model on a more physics-informed approach; the more neighbors an atom has the weaker the bonds will be. Thus, it introduces the bond order (bond strength), which is environment specific and decreases with increasing bond coordination (number of neighbors for a given atom). A sketch of the Tersoff potential can be seen in Fig. 2.3.

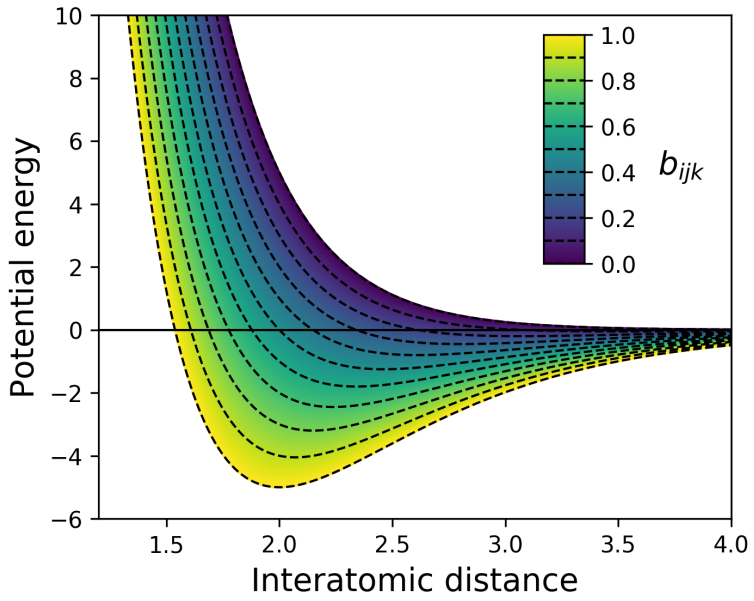

Figure 2.3: Sketch of the potential energy for a Tersoff-type potential. The energy minimum is shifted with changing bond order b_{ijk}. Reproduced from [41].

The potential energy is taken to have the form

$$U = \sum_i U_i = \frac{1}{2}\sum_{i \neq j} V_{ij},$$
$$V_{ij} = f_C(r_{ij})\big[f_R(r_{ij}) + b_{ij} f_A(r_{ij})\big],$$

where the total potential energy U is decomposed into a bond energy V_{ij}. The indices i and j run over the atoms of the system with r_{ij} denoting the distance between atom i and j. Notice that the sum includes all combinations of i, j but $i \neq j$, meaning that an atom cannot bond to itself. However, we count other bonds twice, e.g. $(1, 2)$ and $(2, 1)$, which is the explanation for the additional factor $1/2$. The reasoning for the double counting lies in the asymmetry of the bond order $b_{ij} \neq b_{ji}$ leading to $V_{ij} \neq V_{ji}$. The bond energy is composed of a repulsive term f_R, arising from overlapping wave functions, and an attractive term f_A associated with bonding. f_C is simply a smooth cut-off function to increase computational efficiency. b_{ij} represent the bond order, i.e. the strength of the bonds, which depends inversely on the number of bonds, the bond angles (θ_{ijk}) and optionally the relative bond lengths (r_{ij}, r_{jk}). Notice that an additional cut-off term a_{ij} was originally multiplied to f_R as a way of limiting the range of the repulsive interactions to the first neighbor shell. This is similar to the role of b_{ij} for the attractive term f_A, but it is often omitted for the repulsive term f_R, and we do so as well by setting $a_{ij} = 1$.

The cut-off function f_C goes from 1 to 0 over a small interval range $R \pm D$ as

$$f_C(r) = \begin{cases} 1 & r < R - D \\ \frac{1}{2} - \frac{1}{2}\sin\left(\frac{\pi}{2}\frac{r-R}{D}\right) & R - D < r < R + D \\ 0 & r > R + D \end{cases},$$

which is continuous and differentiable for all r. R is usually chosen to include only the first neighbor shell. The repulsive and attractive terms f_R and f_A are modeled as an exponential function, similar to a Morse potential,

$$f_R(r) = A\exp(-\lambda_1 r),$$
$$f_A(r) = -B\exp\big(-\lambda_2 r\big).$$

The novel feature of the Tersoff model lies in the modeling of the bond order b_{ij} which includes three-body interactions by summing over a third atom $k \neq i, j$ within the cut-off $r_{ik} < R + D$ as shown in the following.

$$b_{ij} = \left(1 + \beta^n \zeta_{ij}^n\right)^{-\frac{1}{2n}} \tag{2.4}$$
$$\zeta_{ij} = \sum_{k \neq i,j} f_C(r_{ik}) g\Big(\theta_{ijk}\left(r_{ij}, r_{ik}\right)\Big) \exp\left(\lambda_3{}^m \big(r_{ij} - r_{ik}\big)^m\right) \tag{2.5}$$
$$g(\theta) = \gamma_{ijk}\left(1 + \frac{c^2}{d^2} - \frac{c^2}{\left[d^2 + (\cos\theta - \cos\theta_0)^2\right]}\right). \tag{2.6}$$

In Eq. (2.6) $\zeta_{i,j}$ is an effective coordination and $g(\theta)$ captures angle dependency and is minimized at the equilibrium angle $\theta = \theta_0$. The parameters used to model the graphene C–C bonds are adopted from J. Tersoff [42] and summarized in Table 2.2.

Table 2.2: Parameters for the Tersoff potential used for intermolecular interactions in the graphene sheet. The parameters are adopted from [42].

Parameter	Value	Description
R	1.95 Å	Center distance for cut-off.
D	0.15 Å	Thickness of cut-off region.
λ_1	3.4879 Å^{-1}	Decay of repulsion potential term f_R.
λ_2	2.2119 Å^{-1}	Decay of attractive potential term f_A.
A	1393.6 eV	Repulsion potential maximum at the core ($f_R(r_{ij} = 0)$).
B	346.74 eV	Attractive potential minimum at core ($f_A(r_{ij} = 0)$).
β	1.5724×10^{-7}	Base for the exponetial scaling of the effective coordination effect on bond strength b_{ij}.
n	0.72751	Power law exponent for the bond order dependency.
λ_3	0.0 Å^{-1}	Base for the exponential cut-off of the effective coordination ζ_{ij}.
m	—	Exponent for the exponential cut-off of the effective coordination ζ_{ij}. Not relevant since $\lambda_3 = 0$.
γ	1.0	Linear scaling of the angle dependecny term.
c	3.8049×10^4	Strength of the angular effect.
d	4.3484	Determines the "sharpness" of the angular dependency.
$\cos(\theta_0)$	−0.57058	Cosine of the equilibrium angle.

2.2 Integration

Assuming that one has defined a system of atoms, defining the atom types, initial positions and velocities, and interatomic potentials, we need to move the system forward in time. By solving Newton's equations of motion we achieve this by effectively sampling the microcanonical ensemble characterized by a constant number of particles N, volume V and energy E, hence denoted NVE [43]. Newton's equations of motion read

$$m_i \frac{d^2\mathbf{r}_i}{dt^2} = \mathbf{F}_i = -\nabla U_i, \tag{2.7}$$

where i is the atom index, m_i its mass, $\mathbf{r}_i = (x_i, y_i, z_i)$ the position, t is time, $\nabla_i = (\frac{\partial}{\partial x_i}, \frac{\partial}{\partial y_i}, \frac{\partial}{\partial z_i})$ and U_i the potential energy. The potential energy is defined by the interatomic potentials and any external forces applied to the system. Since the forces defined by the potentials are conservative we expect the energy of the solution to be conserved. We can redefine Eq. (2.7) in terms of two coupled first order differential equations

$$\dot{\mathbf{v}}_i(t) = \frac{\mathbf{F}}{m_i}, \qquad \dot{\mathbf{r}}_i(t) = \mathbf{v}_i(t), \tag{2.8}$$

where $\dot{x} = dx/dt$ is Newton's notation for the time derivative and $\mathbf{v} = (v_x, v_y, v_z)$ is velocity. Numerically we can solve the coupled equations by integrating over discrete timesteps. That is, we discretize the solution into temporal steps $t_k = t_0 + k\Delta t$ with start time t_0 and timestep Δt. The choice of timestep should be chosen small enough to avoid instabilities in the numerical solution.

2.2.1 Velocity Verlet

A popular approach to the numerical integration of Newton's equations of motion, when written as two coupled first-order differential equations Eq. (2.8), is the *velocity verlet* algorithm. We can derive the algorithm by the use of Taylor expansions. We begin by expanding the next-step position vector $\mathbf{r}_i(t + \Delta t)$ at time t

$$\mathbf{r}_i(t + \Delta t) = \mathbf{r}_i(t) + \dot{\mathbf{r}}_i(t)\Delta t + \frac{\ddot{\mathbf{r}}_i(t)}{2}\Delta t^2 + \mathscr{O}(\Delta t^3), \tag{2.9}$$

where $\ddot{\mathbf{r}} = d^2\mathbf{r}/dt^2$ and Δt^n is simply the relaxed notation for $(\Delta t)^n$. The remaining $\mathscr{O}(\Delta t^3)$ term is big O notation for the truncation including a dependence of Δt^3 and higher order. Similarly, we take the expansions of

the next-step velocity vector $\mathbf{v}_i(t+\Delta t)$ at time t

$$\mathbf{v}_i(t+\Delta t) = \mathbf{v}_i(t) + \dot{\mathbf{v}}_i(t)\Delta t + \frac{\ddot{\mathbf{v}}_i(t)}{2}\Delta t^2 + \mathscr{O}(\Delta t^3). \tag{2.10}$$

Finally, by taking the expansion of $\dot{\mathbf{v}}_i(t+\Delta t)$ we can eliminate the $\ddot{\mathbf{v}}_i$-term in Eq. (2.10) and simplify it as shown in the following.

$$\begin{aligned}
\dot{\mathbf{v}}_i(t+\Delta t) &= \dot{\mathbf{v}}_i(t) + \ddot{\mathbf{v}}_i(t)\Delta t + \mathscr{O}(\Delta t^2) \\
\frac{\ddot{\mathbf{v}}_i(t)}{2}\Delta t^2 &= \frac{\Delta t}{2}\Big(\dot{\mathbf{v}}(t+\Delta t) - \dot{\mathbf{v}}_i(t)\Big) + \mathscr{O}(\Delta t^3) \\
&\Downarrow \\
\mathbf{v}_i(t+\Delta t) &= \mathbf{v}_i(t) + \dot{\mathbf{v}}_i(t)\Delta t + \frac{\Delta t}{2}\Big(\dot{\mathbf{v}}_i(t+\Delta t) - \dot{\mathbf{v}}_i(t)\Big) + \mathscr{O}(\Delta t^3) \\
&= \mathbf{v}_i(t) + \frac{\Delta t}{2}\Big(\dot{\mathbf{v}}_i(t) + \dot{\mathbf{v}}_i(t+\Delta t)\Big) + \mathscr{O}(\Delta t^3).
\end{aligned} \tag{2.11}$$

By combining Eq. (2.9) and Eq. (2.11) using $\dot{\mathbf{v}} = \mathbf{F}_i(t)/m_i$ and $\mathbf{v} = \dot{\mathbf{r}}$ we arrive at the final scheme

$$\begin{aligned}
\mathbf{r}_i(t+\Delta t) &= \mathbf{r}_i(t) + \mathbf{v}_i(t)\Delta t + \frac{\mathbf{F}_i(t)}{2m_i}\Delta t^2 + \mathscr{O}(\Delta t^3), \\
\mathbf{v}_i(t+\Delta t) &= \mathbf{v}_i(t) + \frac{\mathbf{F}_i(t) + \mathbf{F}_i(t+\Delta t)}{2m_i}\Delta t + \mathscr{O}(\Delta t^3).
\end{aligned}$$

This scheme will give a local error on the order Δt^3 corresponding to a global error of Δt^2. One of the most popular ways to implement this numerically is as stated in the following steps.

1. Calculate $v_{k+\frac{1}{2}} = v_k + \frac{F_k}{2m}\Delta t$.
2. Calculate $r_{k+1} = r_k + v_{k+\frac{1}{2}}\Delta t$.
3. Evaluate the force $F_{k+1} = F(r_{k+1})$.
4. Calculate $v_{k+1} = v_{k+\frac{1}{2}} + \frac{F_{k+1}}{2m}\Delta t$

2.3 Thermostats

In **??** we introduced friction as an ultimate result of the equipartition theorem stating that the kinetic energy supplied by the sliding motion will tend to transfer to other degrees of freedom and eventually dissipate to the environment as heat through phonon transport (and electrons for a metallic system) [25]. However, when modeling the system exclusively through the solutions of Newton's equations of motion we have no dissipation channel in our system. Instead, the energy will reflect back and forth and eventually "pile up" in the system in an unphysical manner. In order to resolve this issue we have to model the heat dissipation to the environment. This can be approached in a variety of ways, but one of the more common choices, which we will use as well, is the Langevin thermostat.

2.3.1 Langevin thermostat

The Langevin thermostat is a stochastic thermostat that modifies Newton's equation of motion such that the solution lies in the canonical ensemble characterized by a constant number of particles N, constant volume V and constant temperature T, hence denoted NVT [25]. When going from the microcanonical ensemble NVE, described by Newton's equation of motion Eq. (2.7), to the canonical ensemble NVT, we effectively perform a Legendre transformation which substitutes temperature for energy in the regard to which variables are held constant. The canonical ensemble is represented by a finite system being in contact with an infinite heat bath of temperature T. The NVT ensemble is equivalent to sampling a system in thermodynamic equilibrium where the weight of each microscopic state is given by the Boltzmann factor $\exp[-E/(k_B T)]$ where k_B is the Boltzmann constant.

The Langevin thermostat is governed by the Langevin equation which originated as the modified version of Newton's equations for a Brownian particle [44]. A Brownian particle is a small particle suspended in liquid, e.g. pollen or dust, named after Robert Brown (1773–1858) who was the first to observe its jittery motion. The Langevin equation describes this motion as the combination of a viscous drag force $-\alpha\mathbf{v}$, where α is a positive friction coefficient and $\mathbf{v}$ the velocity vector, and a random fluctuation force $\mathbf{R}$. The Langevin equation reads

$$m\frac{d\mathbf{v}}{dt} = -\alpha\mathbf{v} + \mathbf{R}, \tag{2.12}$$

where m is the particle mass. This effectively describes the particle of interest, the Brownian particle, as being suspended in a sea of smaller particles. The collision with these smaller particles is modeled by the combined effects of the drag force and the fluctuation force. If the fluctuation force is excluded Eq. (2.12) becomes

$$m\frac{d\mathbf{v}}{dt} = -\alpha\mathbf{v} \quad \Rightarrow \quad \mathbf{v}_i(t) = v(0)e^{-\frac{\alpha t}{m}},$$

where the solution reveals that the Brownian particle will come to a complete stop after a long time $\mathbf{v}_i(t \to \infty) \to \mathbf{0}$. This is in violation with the equipartition theorem which dictates a non-zero average squared velocity in equilibrium $\langle v^2 \rangle_{\text{eq}}$ as

$$\frac{1}{2}m\langle v^2 \rangle_{\text{eq}} = \frac{k_B T}{2}. \tag{2.13}$$

Hence, the fluctuation force is necessary to obtain the correct equilibrium. In the following, we will attempt to introduce the reasoning behind the Langevin equations using only one dimension in order to simplify the notation a bit. This is based on [44].

We describe the statistical nature of the collisions as a sum of independent momentum transfers

$$\Delta P = \sum_i^N \delta p_i,$$

where ΔP denotes the change of momentum after N momentum transfers δp_i from the environment to the Brownian particle. We assume the first and second moments to be $\langle \delta p \rangle = 0$ and $\langle \delta p \rangle = \sigma^2$. When N is large the central limit theorem states that the random variable ΔP has a gaussian distribution with $\langle P \rangle = 0$ and $\langle \Delta P^2 \rangle = N\sigma^2$. If we consider the momentum change ΔP over a discrete time Δt, where the number of collisions is proportional to time $N \propto \Delta t$, the corresponding fluctuation force $R = \Delta P/\Delta t$ will have a variance

$$\langle R^2 \rangle = \frac{\langle \Delta P^2 \rangle}{\Delta t^2} = \frac{N\sigma^2}{\Delta t^2} \propto \frac{1}{\Delta t}.$$

In an MD simulation, we pick a random force $R(t)$ from a Gaussian distribution every timestep Δt. These forces will not be correlated as long as Δt is larger than the correlation time of the forces from the molecular fluid. By assuming that this criterion is met we can write the correlation function as

$$\langle R(t)R(0) \rangle = \begin{cases} \frac{a}{\Delta t}, & |t| < \Delta t/2 \\ 0, & |t| > \Delta t/2, \end{cases} \tag{2.14}$$

where the constant a describes the magnitude of the fluctuations. We could in principle determine a from the variance of ΔP, but instead, we will determine it from the equipartition principle. In the limit $\Delta t \to 0$ the correlation function becomes

$$\langle R(t)R(0) \rangle = a\delta(t), \tag{2.15}$$

where δ denotes the Dirac delta function. This is valid for all spatial coordinates which are all independent of each other. Since both the drag force and the fluctuation force originate from the molecular fluid, where the drag force $-\alpha\mathbf{v}$ carries a velocity dependency, it is reasonable to assume that fluctuation force is independent of velocity, i.e. $\langle R_i v_j \rangle = 0$ for all cartesian indices i and j. In the following, we attempt to justify the physical motivation for the Langevin equation by determining the relationship between the drag coefficient α and the

random force R [44]. From the Langevin equation Eq. (2.12) we can compute the velocity autocorrelation function. Note that we continue to use only one dimension for simplicity. We begin by multiplying by $(e^{\alpha t/m})/m$

$$\dot{v}(t)e^{\alpha t/m} + \frac{\alpha}{m}v(t)e^{\frac{\alpha t}{m}} = \frac{F}{m}e^{\frac{\alpha t}{m}}.$$

We integrate from $t = -\infty$, using integration by parts on the latter term on the left-hand side, in order to calculate the velocity

$$\int_{-\infty}^{t} dt'\ \dot{v}(t')e^{\frac{\alpha t'}{m}} + \frac{\alpha}{m}v(t)e^{\frac{\alpha t'}{m}} = \int_{-\infty}^{t} dt'\ e^{\frac{\alpha t'}{m}}\frac{F(t')}{m}$$

$$\int_{-\infty}^{t} dt'\ \dot{v}(t')e^{\frac{\alpha t'}{m}} + \left(\left[v(t')e^{\frac{\alpha t'}{m}}\right]_{-\infty}^{t} - \int_{-\infty}^{t} dt'\ \dot{v}(t')e^{\frac{\alpha t'}{m}}\right) = \int_{-\infty}^{t} dt'\ e^{\frac{\alpha t'}{m}}\frac{F(t')}{m}$$

$$v(t) = \int_{-\infty}^{t} dt'\ e^{\frac{-\alpha(t-t')}{m}}\frac{F(t')}{m},$$

where $e^{\frac{-\alpha t}{m}}$ plays the role of a response function. We can then calculate the autocorrelation

$$\begin{aligned}\langle v(t)v(0)\rangle &= \int_{-\infty}^{t} dt_1 \int_{-\infty}^{0} dt_2\ e^{\frac{t-t_1-t_2}{m}}\frac{\langle F(t_1)F(t_2)\rangle}{m^2}\\ &= \int_{-\infty}^{t} dt_1 \int_{-\infty}^{0} dt_2\ e^{\frac{t-t_1-t_2}{m}}\frac{a\delta(t_1-t_2)}{m^2}\\ &= \int_{-\infty}^{0} dt_2\ e^{\frac{t-2t_2}{m}}\frac{a}{m^2} = \frac{a}{2m\alpha}e^{-\frac{\alpha t}{m}},\end{aligned}$$

where we used Eq. (2.15) and the fact that the integration commutes with the average (we are allowed to flip the order). By comparing this with the equipartition theorem we get

$$\frac{1}{2}m\langle v^2\rangle = \frac{k_BT}{2}$$

$$\frac{1}{2}m\langle v(0)v(0)\rangle = \frac{a}{4\alpha} = \frac{k_BT}{2}$$

$$a = 2\alpha k_BT$$

We notice the appearance of α meaning that the magnitude of the fluctuations increase both with viscous friction $(-\alpha\mathbf{v})$ and temperature T. Moreover, we can integrate the velocity over time to get displacement $x(t)$ and show that the variance is [44]

$$\langle x^2(t)\rangle = \frac{2k_BT}{\alpha}\left(t - \frac{m}{\alpha}\left(1 - e^{-\alpha t/m}\right)\right).$$

For $t \gg m/\alpha$, only the t-term will survive yielding

$$\langle x^2(t)\rangle = 2k_BTt/\alpha.$$

In 1D, the diffusion constant D is related to the variance as $\langle x^2\rangle = 2Dt$, meaning that this represents the Einstein relation $D = \mu k_BT$ with the mobility $\mu = 1/\alpha$. When $t \ll m/\alpha$, we use the Taylor expansion $1 - e^{-x} \approx x - x^2/2$ for $x \ll 1$ which gives

$$\langle x^2(t)\rangle = \frac{k_BT}{m}t^2.$$

Using $\langle x^2\rangle/t^2 = \langle v^2\rangle$ we see that the result is in agreement with the equipartition theorem Eq. (2.13)

$$\langle v^2(t)\rangle = \frac{k_BT}{m} \iff \frac{1}{2}m\langle v^2\rangle_{\text{eq}} = \frac{k_BT}{2}.$$

Thus, we find the finite correlation time α/m to describe the crossover from the ballistic regime $\sqrt{\langle x^2(t)\rangle} \propto \sqrt{t}$ at $t \ll m/\alpha$ to the diffusive regime $\sqrt{\langle x^2(t)\rangle} \propto \sqrt{t}$ at $t \gg m/\alpha$. That is, at short time scales the thermal movement can be thought of as relatively free with a low collision rate, while at longer time scales the movement is characterized by a jittery random-walk-looking motion that is related to diffusion.

2.3.2 Implementing Langevin

The numerical implementation of the Langevin equation Eq. (2.12) is done through the simulation software LAMMPS (see Sec. 2.5) following [45] by defining the force vector for each particle as

$$\begin{aligned}\mathbf{F} &= \mathbf{F_c} + \mathbf{F}_f + \mathbf{F}_r \\ &= -\nabla U - \gamma m \mathbf{v} + \sqrt{\frac{2k_B T m\gamma}{\Delta t}}\mathbf{h}(t)\end{aligned} \tag{2.16}$$

where $\mathbf{F_c}$ is the added conservative force computed via the usual interatomic interactions described by the potential U, $\mathbf{F}_f$ is the drag force described as a damping term $-\gamma m\mathbf{v}$ with $\alpha = \gamma m$, and $\mathbf{F}_r$ is the random fluctuation force where $\mathbf{h}$ is a random vector drawn from a normal distribution with zero mean and unit variance. The fact that Δt now appears in the denominator for the random force variance $2k_BTm\gamma/\Delta t$ is due to the discretization of time. By applying Eq. (2.16) we get the refined velocity verlet scheme

$$\begin{aligned}\mathbf{v}_i(t+\Delta t/2) &= \mathbf{v}_i(t) - \frac{\Delta t}{2}\left(\frac{\nabla_i U(t)}{m_i} + \gamma \mathbf{v}_i\right) + \sqrt{\frac{k_B T\gamma \Delta t}{2m_i}}\mathbf{h}_i \\ \mathbf{r}_i(t+\Delta t) &= \mathbf{r}_i(t) + \mathbf{v}_i(t+\Delta t/2)\Delta t \\ \mathbf{v}_i(t+\Delta t) &= \mathbf{v}_i(t+\Delta t/2) - \frac{\Delta t}{2}\left(\frac{\nabla_i U(t+\Delta t)}{m_i} + \gamma \mathbf{v}_i(t+\Delta t/2)\right) + \sqrt{\frac{k_B T\gamma \Delta t}{2m_i}}\mathbf{h}_i\end{aligned}$$

with new random vector $\mathbf{h}_i$ for each particle and each update. Notice however, we will only apply the thermostat to specific regions in our simulation, mainly on the outer edges, while the main part of interest is modeled exclusively by Newton's equation of motion as described in Eq. (2.7). This is done in order to avoid affecting the governing parts of the friction simulation to much. We use a damping of $1/\gamma = m/\alpha = 1\,\text{ps}$ as a common default choice.

2.4 Limitations

On a general note, MD simulations are limited to relatively small time and size scales due to the available computation time. Morden CPUs perform on the order of 10^9 floating-point operations per second (FLOPS) per core [29]. MD simulations can benefit from medium-scale parallelization, demonstrating relatively linear scaling up to around 10^2 cores, providing roughly 10^{11} FLOPS. In a typical MD calculation, the computation of the force acting on each atom, which can be the most time-consuming step depending on the complexity and range of the force field, requires N_{step} steps being approximately 10 to 10^2 FLOPS. Therefore, for a typical simulation size of $N = 10^5$ atoms with a timestep in the fs range, we find the ratio of simulated time to real-time on the order

$$\frac{\text{FLOPS}}{N \cdot N_{\text{step}} \cdot dt^{-1}} \sim \frac{10^{11}}{10^5 \cdot 10 \cdot 10^{15}} = 10^{-10}.$$

Hence, the simulation can make progress at a rate of 100 ps per second, or roughly $10^9\,\text{fs} = 1\,\mu\text{s}$ per day. This serves as a rough estimate for the capabilities of MD simulations. Regarding the "realism" of the simulations, some general weaknesses include the lack of considering quantum effects and a reduction in the number of dissipation channels available.

2.5 LAMMPS

For the implementation of our MD we use LAMMPS (Large-scale Atomic/Molecular Massively Parallel Simulator) [20]. LAMMPS provides a numerical framework for setting up the system and integrating the equations of motion with easy access to parallelization of the simulations. This essentially allows us to focus on the higher-level features of the numerical procedure rather than writing the code from scratch.

Part II

Simulations

Chapter 3

Summary

In this thesis, we have studied the nanoscale friction of a Kirigami graphene sheet under the influence of strain using molecular dynamics (MD) simulations. We have developed a numerical tool for generating diverse Kirigami designs which we have utilized to create a dataset for the frictional behavior depending on Kirigami pattern, strain, and loading. Our findings suggest that the frictional behavior of a Kirigami sheet is highly dependent on the geometry of the pattern and the strain conditions. We observed that the out-of-plane buckling can be associated with a non-linear friction-strain relationship which can be utilized to demonstrate a negative friction coefficient in a system with coupled load and strain. Moreover, we have investigated the possibility to use machine learning on this dataset and we have attempted an accelerated search for the optimization of various friction properties. Our findings imply that machine learning can be feasible for this approach, but additional data is required to establish a more reliable foundation for the prediction on new Kirigami patterns. In this chapter, we will provide a summary of our findings and draw conclusions based on the results obtained. Finally, we will suggest some topics for further research.

3.1 Summary and conclusions

3.1.1 Designing an MD simulation

We have designed an MD simulation for the examination of friction for a graphene sheet sliding on a silicon substrate. The key system features were the introduction of the pull blocks, defined as the end regions of the sheet with respect to the sliding direction, which was utilized for applying normal load and sliding the sheet. The pull blocks were made partly rigid and used to employ a thermostat as well. Through an analysis of the friction forces retrieved from sliding simulations, we have established a standardized metric for kinetic friction. In particular, we measured the force exerted by the substrate on the full sheet, including the pull blocks, with respect to the sliding direction. We then determined the kinetic friction as the force mean value of the last half of the simulation. The uncertainties were estimated based on the fluctuations in the running mean. We found that the assessment of static friction was ambiguous for our simulation and did not pursue this further. From the analysis of the force traces, friction force vs. time, we identify the friction behavior in our simulation domain as being in the smooth sliding regime. This is attributed to the choice of a relatively high sliding speed (20 m/s) and infinitely stiff springs for the tethering of the sheet. This was supported by a demonstration of a transition to the stick-slip regime through the use of softer springs and a decrease in sliding speed. By conducting a more systematic investigation of the effects of temperature, sliding speed, spring constant and timestep, we identified a set of default values based on numerical stability and computational cost. During this process, we aimed to select the variables that would maintain relatively stable measures for friction with moderate perturbations around these default values. We found that friction increased with temperature which is in disagreement with the Prandtl–Tomlinson model and most experimental results. However, this agrees with the predictions from the Frenkel-Kontorova models and other MD studies which attribute this to ballistic sliding. In the absence of clear indications from the investigation regarding an appropriate temperature, we opted for the standard choice of room temperature, 300 K. Furthermore, we found friction to increase with velocity as expected from other studies and the Prandtl–Tomlinson model, with some signs of phonon resonance at certain sliding speeds as well which aligns with the predictions from the Frenkel-Kontorova models. We chose a rather high velocity

of 20 m/s mainly for the consideration of computational costs. For the spring constant, we found decreasing friction with increasing stiffness of the springs. This is associated with the transition from a stick-slip-influenced regime toward smooth sliding and can be attributed to an underlying change in commensurability. This is predicted by the Frenkel-Kontorova models and supported by both numerical and excperimental results. The choice of an infinitely stiff spring was made from an assessment of the variation in friction with perturbations in the spring constant value. Finally, we confirmed that a timestep of 1 fs provides reasonable numerical stability. However, based on fluctuations with timestep we find that the uncertainty in the simulations might be higher than first estimated. For the non-strained Kirigami sheet, these fluctuations were on the order of ± 0.017 nN for the evaluation of the kinetic friction.

3.1.2 Generating Kirigami patterns

In order to investigate the effects of Kirigami design we have created a numerical tool for generating various patterns. By defining an indexing system for the hexagonal lattice structure we were able to define the Kirigami designs as a 2D binary matrix for numerical implementation. We have selected two macroscale designs, which we denote the *Tetrahedron* and *Honeycomb* patterns, based on their ability to exhibit out-of-plane buckling when subjected to strain. By digitalizing the designs to match the hexagonal graphene lattice, we found that the characteristic design features can be translated to the nanoscale, as we observed similar out-of-plane buckling in MD simulations. Through our numerical tool we were able to create an ensemble of perturbed unique variations which yielded approximately 1.35×10^5 and 2.025×10^6 unique configurations for the Tetrahedron and Honeycomb patterns respectively. When considering the possibility to translate the periodic patterns on the sheet, the number of possible patterns can be increased by approximately a factor of 100. To introduce some random design features, we have developed a tool for generating Kirigami patterns based on random walks. The tool includes mechanisms such as bias, avoidance of existing cuts, preference for maintaining a direction, and procedures for repairing the sheet for simulation purposes. In general, we found that the capabilities of the numerical tools for generating Kirigami designs exceeded our computational resources with regard to performing MD simulation under different loads and strains for each of the designs. Our MD-based dataset only utilized a subset of configurations with 9660 data points based on 216 Kirigami configurations (Tetrahedron: 68, Honeycomb: 45, Random walk: 100, Pilot study: 3). Hence, we argue that the Kirigami generative tool can be valuable for further studies on an extended dataset.

3.1.3 Friction control using Kirigami design and strain

We have investigated the frictional behavior of the Tetrahedron and Honeycomb patterns in comparison to a non-cut sheet under various strains and loads. Initially, we observed that straining the Kirigami sheets in a vacuum resulted in an out-of-plane buckling. When adding the substrate to the simulation this translated into a decreasing contact area with strain. We found the Honeycomb sheet to exhibit the most significant buckling with a corresponding reduction of relative contact to approximately 43%, whereas the non-cut sheet did not produce any significant buckling in comparison. For the Kirigami sheets, we found that friction initially increased with strain, which made for increasing friction with decreasing contact area. As the strain continued to increase the friction-strain curve exhibited highly non-linear trends with strong negative slopes as well (see **??**). During the full strain, the contact area was decreasing monotonically except for a slight increase just before rupturing. These results contradict the asperity theory hypothesis of decreasing friction with decreasing contact area, which is also supported by the predictions of the 2D Frenkel-Kontorova models suggesting increasing friction with (contacting) system size. Thus, we conclude that the contact area is not a governing mechanism for the friction-strain relationship observed. From the investigation of the friction-load relationship, we found that both friction and contact area increased slightly with load, but we were not able to find significant evidence of any linear relationship between friction and contact area as predicted by asperity theory. The non-cut sheet did not show any dependency on the strain as both the friction and the contact area remained constant with strain. Thus our findings suggest that a changing contact area and the strain-induced friction effects might be associated with an underlying mechanism related to the buckling of the sheet. When analyzing the independent effect of the non-strained Kirigami sheets, we found a slight increase in friction between the non-cut sheet and the Kirigami sheets. However, this increase was one order of magnitude lower than the friction changes induced by the strain in combination. Therefore, we can conclude that the observed friction behavior cannot be attributed solely to the effects of the non-strained Kirigami sheet or the tension induced by the strain in a non-cut sheet.

When considering the friction dependency with load, we generally found a weak dependency corresponding to a friction coefficient on the order of 10^{-4}–10^{-5} even though we could not confirm any clear relationship. This is best attributed to the superlubric state of the graphene sheet as seen in other studies as well. The slope of the friction-load curve was not considerably affected by the straining of the Kirigami sheet which led us to the conclusion that strain-induced effects are dominant in comparison to any load-related effects.

When considering our findings in light of previous related results we find it plausible that the governing mechanism for the observed friction effects is related to commensurability as predicted by the Frenkel-Kontorova models. Since we have observed extremely low friction in our system, we argue that the non-deformed sheet corresponds to an incommensurable configuration. This is supported by the fact that we were not able to lower the friction below the original starting point. Additionally, this also aligns with the observation that the introduction of the non-strained Kirigami designs increased friction slightly. Since the Kirigami designs correspond to the removal of atoms from the sheet, it can be hypothesized to relax the incommensurability to some extent. When the Kirigami sheet buckles during stretching, it allows for a considerable rearrangement of the atoms in contact with the substrate. Hence, it may transition in and out of commensurable configurations, which could explain the non-linear trend for the friction-strain curve. One way to test this hypothesis is to alter the simulation conditions such that the non-strained sheet starts in a commensurable phase. This might be achieved by a softening of the springs for tethering and a lowering of the sliding speed since this was found to yield stick-slip behavior which can be associated with a commensurable phase. Another way is to reorient the sheet or change the sliding direction as reported in both numerical and experimental results. Then we might find a transition from a commensurable to an incommensurable case during the initial straining which would result in a lowering in friction with respect to the starting point.

3.1.4 Capturing trends with machine learning

By utilizing the numerical tool for generating Kirigami designs we have created a MD-based dataset for the frictional behavior depending on Kirigami design, load and strain. The dataset reveals some general correlations with mean friction, such as a positive correlation to strain (0.77) and porosity (0.60), and a negative correlation to contact area (-0.67). These results align with the finding in the pilot study, suggesting that the change in friction is associated with cuts in the sheet (porosity) and a changing contract area indicating out-of-plane buckling.

By defining the friction property metrics: $\min F_{\text{fric}}$, $\max F_{\text{fric}}$, $\max \Delta F_{\text{fric}}$ and max drop (maximum decrease in friction with strain), we investigated the top design candidates within our dataset. From these results, we found no indication of the possibility to reduce friction with the Kirigami approach since the non-cut sheet provided the overall lowest friction. Furthermore, among the top candidates, we found that a flat friction-strain profile is mainly associated with little decrease in the contact area and vice versa. These observations are consistent with the results of the pilot study and support the hypothesis that commensurability plays a key role in governing the behavior of the system. In terms of the maximum properties, we observed an improvement compared to the values obtained in the pilot study, with the Honeycomb patterns exhibiting the highest scores. This indicates that the dataset contains some relevant information for optimizing these properties since it includes examples of design improvements.

For the machine learning investigation, we have implemented a VGGNet-inspired convolutional neural network with a deep "stairlike" architecture: C32-C64-C128-C256-C512-C1024-D1024-D512-D256-D128-D64-D32, for convolutional layers C with the number denoting channels and fully connected (dense) layers D with the number denoting nodes. The final model contains 1.3×10^7 parameters and was trained using the ADAM optimizer for a cyclic learning rate and momentum scheme. We trained the network for a total of 1000 epochs while saving the best model during training based on the validation score. The model validation performance gives a mean friction R^2 score of $\sim 98\%$ and a rupture accuracy of $\sim 96\%$. However, we got lower scores for a selected subset of the Tetrahedon ($R^2 \sim 88.7\%$) and Honeycomb ($R^2 \sim 96.6$) pattern based on the top 10 max drop property scores respectively. The scores obtained were lower, even though the selected configurations were partly included in the training data and the hyperparameter selection favored the performance on this selected set. Thus we conclude that these selected configurations, associated with a highly non-linear friction-strain curve, represent a bigger challenge for machine learning prediction. One interpretation is that these involve the most complex dynamics and perhaps that this is not readily distinguished from the behavior of the other configurations which constitute the majority of the dataset. By evaluating the ability of the model to rank the dataset based on property scores, we found that it was able to effectively represent the top three scores for the maximum categories.

However, the ranking for the minimum friction property was lacking, which we attribute to the requirement of higher prediction precision that the model did not meet To obtain a more accurate evaluation of the model's performance, we generated a test set using MD simulations for some of the random walk based suggestions obtained from the accelerated search. The results showed a significantly worse performance compared to the validation set, with a two-order of magnitude higher loss and a negative R^2 score for the mean friction property. The negative R^2 score suggests that the model's predictions were worse than simply predicting the mean value of the true data. However, by reevaluating the hypertuning and choosing solely based on validation loss, we still found poor results on the test set. This suggests that the inadequate performance is not solely due to a biased hypertuning process, but rather because our original dataset did not cover a sufficiently diverse range of Kirigami configurations. The validation scores indicate that the use of machine learning is a feasible approach for addressing this problem, as we were able to identify some general trends in the data. Nonetheless, from the test scores, it is evident that further improvements to the dataset are necessary in order to develop a reliable model.

3.1.5 Accelerated search for Kirigami patterns

Using the machine learning model we performed two types of accelerated search. One by evaluating the property scores of an extended dataset and another with the use of the genetic algorithm approach. For the extended dataset search, we used the developed pattern generators to generate 1.35×10^6 Tetrahedron, 2.025×10^7 Honeycomb and 10^4 Random walk patterns. The search results for the minimum friction property indicate a preference for low cut density. This aligns with the overall observation that the dataset does not provide any suggestions for a further reduction in friction.

The search for the maximum properties resulted in some minor score increases, but the suggested candidates were mainly overlapping with the original dataset. By investigating the sensitivity to translations of the Tetrahedron and Honeycomb patterns, we observed significant variations in the model's predictions with only minor translations. This can be attributed to a physical dependency since these translations affect the edge of the sheet. However, given the poor model performance on the test set, we believe it is more likely that this variation is due to an insufficiency in the model caused by the limitations of the dataset.

In our investigation of the genetic algorithm approach, we used a starting population that was based on the results from the extended dataset accelerated search, as well as some randomly generated initializations with different porosity values. However, this approach did not provide any noteworthy indication for new design structures worth more investigation. In general, the initialization of the population itself proved to be a more promising strategy than the genetic algorithm. We acknowledge that further effort could potentially yield useful results with the genetic algorithm approach. However, we believe that the current lack of promising results can be attributed to the uncertainty of the model which where the reason for not pursuing this any further.

By considering the Grad-CAM explanation method, we observed that the model predictions were often substantially reliant on the top and bottom edges of the Kirigami configurations. This was unexpected since these edges are not true edges but are connected to the pull blocks used in the simulation. Despite the model's uncertain predictions, we speculate that this may be due to the thermostat effects from the pull blocks. Therefore, we note this as a feature worth investigating in the simulations.

3.1.6 Negative friction coefficient

Based on our initial investigations of the Kirigami sheet, we have discovered a highly non-linear friction-strain relationship. By proposing a linear coupling between load and strain with ratio R, we found that these results suggest the possibility to utilize the negative slope on the friction-strain curve to achieve a negative friction coefficient. Based on the decrease in friction from the top to bottom of these curves, using the Tetrahedron $(7, 5, 1)$ and Honeycomb $(2, 2, 1, 5)$ pattern from the pilot study, we estimate that the average coefficient within this range will be $-R12.75\,\mathrm{nN}$ for the Tetrahedron pattern and $-R \cdot 2.72\,\mathrm{nN}$ for the Honeycomb pattern.

To investigate this hypothesis, we conducted a simulation with a coupling between load and sheet tension, mimicking a nanomachine attached to the sheet, using the Kirigami configurations from the Pilot study. We observed that the non-linear behavior in the friction-strain curve also translated into a non-linear friction-load relationship for the coupled system. Additionally, we found that the Honeycomb pattern exhibited a non-linear strain-tension curve which resulted in an almost discontinuous increase in friction for the initial increase in load. We attribute this feature to an unfolding process visually confirmed from the simulation frames. For the coupled system with a load-to-tension ratio of 6, we found regions in the friction-load curve with significant negative

slopes. By considering the maximum and minimum points for such regions we estimated the average friction coefficient to be -0.31 in the load range $F_N = [4.65, 6.55]$ nN for the Tetrahedron pattern and -0.38 in the range $F_N = [0.71, 4.31]$ nN for the Honeycomb pattern. These results can be scaled by adjusting the load-to-tension ratio.

Based on our investigations, we have found that the combination of Kirigami cuts and strain has significant potential for controlling friction. Specifically, we have demonstrated that by enforcing a coupling between load and strain through tension, it is possible to achieve a negative friction coefficient. Therefore, we believe that this approach could be promising for developing novel friction-control strategies.

3.2 Outlook

In this thesis, we have demonstrated that certain Kirigami designs exhibit non-linear friction behavior with strain. This discovery was made through an exploration of different designs, which invites further investigation into the underlying mechanisms of this phenomenon. To this end, it would be valuable to choose only one or two selected designs, such as the Tetrahedron and Honeycomb patterns, and study the effects of various physical parameters on the friction-strain curve.

First of all, we suggest an investigation of how the friction-strain curve depends on temperature, sliding speed, spring constant, and loads for an increased range $F_N > 100nN$. This is especially interesting in the context of physical conditions leading to a stick-slip behavior since our study takes a basis in smooth sliding friction. Moreover, it would be valuable to verify that the choices for relaxation time, pauses, interatomic potentials and substrate material are not critical for the qualitative observations found for the friction-strain relationship. Especially the Adaptive Intermolecular Reactive Empirical Bond Order (AIREBO) potential for the modeling of the graphene sheet might be of interest. In this context, it might also be useful to investigate the effects of excluding adhesion from the simulations.

In order to investigate the hypothesis of commensurability as a governing mechanism we suggest an investigation of the friction-strain curve for different scan angles. If commensurability is an important factor, we hypothesize that the friction-strain curve will exhibit different qualitative shapes at varying scan angles. Additionally, it may be interesting to investigate the friction-strain relationship under a uniform load to gain insight into how the loading distribution affects the out-of-plane buckling and associated commensurability effect.

Another topic worth exploring is the impact of scale and edge effects. This includes an investigation of scaling the ratio of the sheet area to the sheet edge length. However, the machine learning predictions also suggest a study of Kirigami-induced edge effects as we translate the patterns on the sheet. With this regard, we would also suggest a more detailed study of the effect of the thermostat in the pull blocks which is suggested to have a possible importance when judging from the Grad-CAM analysis.

Regarding the machine learning approach, our findings indicate that there is a significant need to expand the dataset. In order to get more insight into this issue one could use unsupervised clustering techniques like the t-Distributed Stochastic Neighbor Embedding (t-SNE) to visualize the distribution of Kirigami configurations in the dataset. Another valuable approach is the active learning method similar to that used by Hanakata et al. [6]. That is, we extend the dataset using the top candidates of a machine learning-driven accelerated search and repeat the process of training the model, searching for new candidates and extending the dataset. This provides a direction for the extension of the dataset which could lead to a more efficient approach to address the dataset problem. We note that one can also create a dataset based on a fixed Kirigami design and vary the physical parameters to support the investigations mentioned above. For both variations, we believe that the results could benefit from a consideration of more advanced model architectures and machine learning techniques. For instance, we suggest increasing the receptive field in the convolutional part of the model, by the use of bigger strides or dilated convolution. If we can develop a reliable machine learning model, it would invite further studies of inverse design methods such as GAN or diffusion models.

Appendices

Bibliography

[1]E. Gnecco and E. Meyer, *Elements of friction theory and nanotribology* (Cambridge University Press, 2015).

[2]Bhusnan, "Introduction", in *Introduction to tribology* (John Wiley & Sons, Ltd, 2013) Chap. 1, 1–?

[3]H.-J. Kim and D.-E. Kim, "Nano-scale friction: a review", International Journal of Precision Engineering and Manufacturing **10**, 141–151 (2009).

[4]K. Holmberg and A. Erdemir, "Influence of tribology on global energy consumption, costs and emissions", Friction **5**, 263–284 (2017).

[5]B. Bhushan, "Gecko feet: natural hairy attachment systems for smart adhesion – mechanism, modeling and development of bio-inspired materials", in *Nanotribology and nanomechanics: an introduction* (Springer Berlin Heidelberg, Berlin, Heidelberg, 2008), pp. 1073–1134.

[6]P. Z. Hanakata, E. D. Cubuk, D. K. Campbell, and H. S. Park, "Accelerated search and design of stretchable graphene kirigami using machine learning", Phys. Rev. Lett. **121**, 255304 (2018).

[7]P. Z. Hanakata, E. D. Cubuk, D. K. Campbell, and H. S. Park, "Forward and inverse design of kirigami via supervised autoencoder", Phys. Rev. Res. **2**, 042006 (2020).

[8]L.-K. Wan, Y.-X. Xue, J.-W. Jiang, and H. S. Park, "Machine learning accelerated search of the strongest graphene/h-bn interface with designed fracture properties", Journal of Applied Physics **133**, 024302 (2023).

[9]Y. Mao, Q. He, and X. Zhao, "Designing complex architectured materials with generative adversarial networks", Science Advances **6**, eaaz4169 (2020).

[10]Z. Yang, C.-H. Yu, and M. J. Buehler, "Deep learning model to predict complex stress and strain fields in hierarchical composites", Science Advances **7**, eabd7416 (2021).

[11]A. E. Forte, P. Z. Hanakata, L. Jin, E. Zari, A. Zareei, M. C. Fernandes, L. Sumner, J. Alvarez, and K. Bertoldi, "Inverse design of inflatable soft membranes through machine learning", Advanced Functional Materials **32**, 2111610 (2022).

[12]S. Chen, J. Chen, X. Zhang, Z.-Y. Li, and J. Li, "Kirigami/origami: unfolding the new regime of advanced 3D microfabrication/nanofabrication with "folding"", Light: Science & Applications **9**, 75 (2020).

[13]OpenAI, *Dall-e2*, 2023.

[14]Midjourney, *Midjourney*, 2023.

[15]Z. Deng, A. Smolyanitsky, Q. Li, X.-Q. Feng, and R. J. Cannara, "Adhesion-dependent negative friction coefficient on chemically modified graphite at the nanoscale", Nature Materials **11**, 1032–1037 (2012).

[16]B. Liu, J. Wang, S. Zhao, C. Qu, Y. Liu, L. Ma, Z. Zhang, K. Liu, Q. Zheng, and M. Ma, "Negative friction coefficient in microscale graphite/mica layered heterojunctions", Science Advances **6**, eaaz6787 (2020).

[17]D. Mandelli, W. Ouyang, O. Hod, and M. Urbakh, "Negative friction coefficients in superlubric graphite–hexagonal boron nitride heterojunctions", Phys. Rev. Lett. **122**, 076102 (2019).

[18]R. W. Liefferink, B. Weber, C. Coulais, and D. Bonn, "Geometric control of sliding friction", Extreme Mechanics Letters **49**, 101475 (2021).

[19]M. Metzsch, *Tuning Frictional Properties of Kirigami Altered Graphene Sheets using Molecular Dynamics and Machine Learning*.

[20]A. P. Thompson, H. M. Aktulga, R. Berger, D. S. Bolintineanu, W. M. Brown, P. S. Crozier, P. J. in 't Veld, A. Kohlmeyer, S. G. Moore, T. D. Nguyen, R. Shan, M. J. Stevens, J. Tranchida, C. Trott, and S. J. Plimpton, "LAMMPS - a flexible simulation tool for particle-based materials modeling at the atomic, meso, and continuum scales", Comp. Phys. Comm. **271**, 108171 (2022).

[21]E. M. Nordhagen, *LAMMPS simulator*.

[22]A. H. Larsen, J. J. Mortensen, J. Blomqvist, I. E. Castelli, R. Christensen, M. Dułak, J. Friis, M. N. Groves, B. Hammer, C. Hargus, E. D. Hermes, P. C. Jennings, P. B. Jensen, J. Kermode, J. R. Kitchin, E. L. Kolsbjerg, J. Kubal, K. Kaasbjerg, S. Lysgaard, J. B. Maronsson, T. Maxson, T. Olsen, L. Pastewka, A. Peterson, C. Rostgaard, J. Schiøtz, O. Schütt, M. Strange, K. S. Thygesen, T. Vegge, L. Vilhelmsen, M. Walter, Z. Zeng, and K. W. Jacobsen, "The atomic simulation environment—a python library for working with atoms", Journal of Physics: Condensed Matter **29**, 273002 (2017).

[23]A. Paszke, S. Gross, F. Massa, A. Lerer, J. Bradbury, G. Chanan, T. Killeen, Z. Lin, N. Gimelshein, L. Antiga, A. Desmaison, A. Kopf, E. Yang, Z. DeVito, M. Raison, A. Tejani, S. Chilamkurthy, B. Steiner, L. Fang, J. Bai, and S. Chintala, "Pytorch: an imperative style, high-performance deep learning library", in *Advances in neural information processing systems 32* (Curran Associates, Inc., 2019), pp. 8024–8035.

[24]Y. Dong, A. Vadakkepatt, and A. Martini, "Analytical models for atomic friction", Tribology Letters **44**, 10.1007/s11249-011-9850-2 (2011).

[25]N Manini, O. M. Braun, E Tosatti, R Guerra, and A Vanossi, "Friction and nonlinear dynamics", Journal of Physics: Condensed Matter **28**, 293001 (2016).

[26]B. Bhushan, "Nanotribology and nanomechanics", Wear **259**, 15th International Conference on Wear of Materials, 1–? (2005).

[27]P. Carloni, U. Rothlisberger, and M. Parrinello, "The Role and Perspective of Ab Initio Molecular Dynamics in the Study of Biological Systems", Accounts of Chemical Research **35**, Publisher: American Chemical Society, 455–464 (2002).

[28]P. Hohenberg and W. Kohn, "Inhomogeneous electron gas", Phys. Rev. **136**, B864–B871 (1964).

[29]A. Vanossi, N. Manini, M. Urbakh, S. Zapperi, and E. Tosatti, "Modeling friction: from nanoscale to mesoscale", Reviews of Modern Physics **85**, 529–552 (2013).

[30]S. Li, Q. Li, R. W. Carpick, P. Gumbsch, X. Z. Liu, X. Ding, J. Sun, and J. Li, "The evolving quality of frictional contact with graphene", Nature **539**, Number: 7630, 541–545 (2016).

[31]J. Tersoff, "New empirical approach for the structure and energy of covalent systems", Phys. Rev. B **37**, 6991–7000 (1988).

[32]P. Zhu and R. Li, "Study of nanoscale friction behaviors of graphene on gold substrates using molecular dynamics", Nanoscale Research Letters **13**, 34 (2018).

[33]Q. Zhang, D. Diao, and M. Kubo, "Nanoscratching of multi-layer graphene by molecular dynamics simulations", Tribology International **88**, 85–88 (2015).

[34]H. M. Yoon, Y. Jung, S. C. Jun, S. Kondaraju, and J. S. Lee, "Molecular dynamics simulations of nanoscale and sub-nanoscale friction behavior between graphene and a silicon tip: analysis of tip apex motion.", Nanoscale **7 14**, 6295–303 (2015).

[35]S. Corporation, *Pair_style lj/cut command*, (Dec. 22, 2022) https://docs.lammps.org/pair_lj.html.

[36]X. Wang, S. Ramírez-Hinestrosa, J. Dobnikar, and D. Frenkel, "The lennard-jones potential: when (not) to use it", Phys. Chem. Chem. Phys. **22**, 10624–10633 (2020).

[37]R. Naeem, *Lennard-jones potential*, (Nov. 25, 2022) https://chem.libretexts.org/Bookshelves/Physical_and_Theoretical_Chemistry_Textbook_Maps/Supplemental_Modules_(Physical_and_Theoretical_Chemistry)/Physical_Properties_of_Matter/Atomic_and_Molecular_Properties/Intermolecular_Forces/Specific_Interactions/Lennard-Jones_Potential.

[38]S. Corporation, *Pair_style sw command*, (Dec. 22, 2022) https://docs.lammps.org/pair_sw.html.

[39]F. H. Stillinger and T. A. Weber, "Computer simulation of local order in condensed phases of silicon", Phys. Rev. B **31**, 5262–5271 (1985).

[40]S. Corporation, *Pair_style tersoff command*, (Dec. 22, 2022) https://docs.lammps.org/pair_tersoff.html.

[41]W. Commons, *File:bond-order interatomic potential.png — wikimedia commons, the free media repository*, [Online; accessed 02/05/2023], 2023.

[42]J. Tersoff, "Modeling solid-state chemistry: interatomic potentials for multicomponent systems", Phys. Rev. B **39**, 5566–5568 (1989).

[43]D. Frenkel and B. Smit, *Understanding molecular simulation: from algorithms to applications*, Second, Vol. 1, Computational Science Series (Academic Press, San Diego, 2002).

[44]F. Ravndal and E. G. Flekkøy, *Statistical physics– a second course*, Department of Physics, University of Oslo, 2019.

[45]T. Schneider and E. Stoll, "Molecular-dynamics study of a three-dimensional one-component model for distortive phase transitions", Phys. Rev. B **17**, 1302–1322 (1978).